Topological invariants of rotationally symmetric crystals

Henke, J.; Kurttutan, M.; Kruthoff, J.; Van Wezel, J.

DOI
10.1103/PhysRevB.104.L201110

Publication date
2021

Document Version
Final published version

Published in
Physical Review B

Letter

Topological invariants of rotationally symmetric crystals

Jans Henke,[1,*] Mert Kurttutan,[1] Jorrit Kruthoff,[2] and Jasper van Wezel[1,†]

[1]*Institute for Theoretical Physics Amsterdam and Delta Institute for Theoretical Physics, University of Amsterdam, Science Park 904, 1098XH Amsterdam, The Netherlands*

[2]*Stanford Institute for Theoretical Physics, Stanford University, Stanford, California 94305, USA*

(Received 7 July 2021; accepted 2 November 2021; published 18 November 2021)

Recent formal classifications of crystalline topological insulators predict that the combination of time-reversal and rotational symmetry gives rise to topological invariants beyond the ones known for other lattice symmetries. Although the classification proves their existence, it does not indicate a way of calculating the values of those invariants. Here we show that a specific set of concentric Wilson loops and line invariants yields the values of all topological invariants in two-dimensional systems with pure rotation symmetry in class AII. Examples of this analysis are given for specific models with twofold and threefold rotational symmetry. We find new invariants that relate to the presence of higher-order topology and corner charges.

DOI: 10.1103/PhysRevB.104.L201110

Introduction. In crystalline topological insulators, the presence or absence of symmetries allows for the emergence of a wide variety of topological phases. These are labeled by an equally wide variety of topological invariants, ranging from the Chern number [1], to the two-dimensional Fu-Kane-Mele (FKM) invariants [2–5], to the Lau-Brink-Ortix (LBO) or line invariants [6], as well as invariant features of the Wilson loop spectrum (WLS) describing higher-order and fragile topological insulators [7–13]. A unified, symmetry-based approach describing all of these topological phases was recently proposed [14–18]. This shows that the FKM, LBO, higher-order, and similar invariants may all be extracted from an algorithmic analysis of lattice symmetries and their effect on the structure of Berry curvature. Moreover, being a complete classification of all possible such invariants (as guaranteed by the underlying K-theory), it predicts that additional, as yet unidentified, invariants of the same type exist in various crystals, for example, those with rotational symmetries in two dimensions [15]. Explicitly, in wallpaper groups $p2$, $p3$, $p4$, and $p6$ we expect to find 4, 2, 3, and 3 $\mathbb{Z}_2$ invariants of which only 3, 1, 2, and 2 invariants are known.

Although the classification predicts the existence of topological invariants for systems with a given symmetry, it does not give a way of identifying or evaluating them in any specific system. Here we introduce a single, unified diagnostic that yields the values of all curvature-based invariants in two-dimensional crystalline topological phases with time-reversal symmetry (TRS) and rotational symmetry, including the new phases predicted by the symmetry-based classification. Our analysis employs a spectrum of concentric Wilson loops rather than the usual spectrum of parallel Wilson loops [4,5,9,10,19]. The concentric loops are tailored to the rotational symmetry of the crystal lattice, allowing them to capture the full influence of symmetry on the topological structure.

We showcase the use of the concentric WLS in examples with threefold and twofold rotational symmetry. We then indicate how the same methodology can be applied to any n-fold rotational symmetry group and discuss the significance of the new invariant with respect to edge and corner states.

The concentric WLS. The gauge invariant eigenvalues of (non-Abelian) Wilson loops can be interpreted as generalizing the (Abelian) Berry curvature to systems with internal and lattice symmetries [7]. We will briefly review the established use of Wilson loops for extracting the FKM invariant before introducing the set of concentric Wilson loops that we employ below to capture the full topology of rotationally invariant crystals.

In a material with N occupied bands, the non-Abelian Berry connection is an $N \times N$ matrix with vector-valued components defined as $\mathbf{A}_{mn}(\mathbf{k}) = i\langle u_m(\mathbf{k})|\nabla_k|u_n(\mathbf{k})\rangle$. Here, $|u_n(\mathbf{k})\rangle$ indicates an occupied Bloch state at momentum $\mathbf{k}$ with band index $n \in \{1, \ldots, N\}$. The Wilson loop $\mathcal{W}[\mathcal{C}]$ on a closed contour $\mathcal{C}$ in the Brillouin zone (BZ) is then given by:

$$\mathcal{W}[\mathcal{C}] = \mathcal{P}\exp\left(i\oint_{\mathcal{C}} d\mathbf{k}\cdot\mathbf{A}\right), \tag{1}$$

with $\mathcal{P}$ indicating path ordering. The Wilson loop is a $U(N)$ matrix and satisfies $\mathcal{W}[\mathcal{C}]\mathcal{W}[\mathcal{C}]^\dagger = \mathcal{W}[\mathcal{C}]\mathcal{W}[\mathcal{C}_r] = 1$, with $\mathcal{C}_r$ the orientation-reversed loop. The Wilson loop can equivalently be expressed as a product of projectors onto the occupied states along the loop, which is particularly convenient when analyzing its properties under symmetry transformations, as shown in Appendix A in Supplemental Material [20].

In systems without any internal or crystal symmetries, one can consistently assign band indices to all states, such that the off-diagonal elements of the Berry connection matrix are zero, and each band can be said to have its own independent Berry curvature and $U(1)$ Wilson loops. The presence of symmetries, however, may cause unavoidable degeneracies between bands, which necessitate the use of the non-Abelian Berry connection. Notably, TRS causes the formation of Kramers

*Corresponding author: j.g.b.henke@uva.nl
†vanwezel@uva.nl

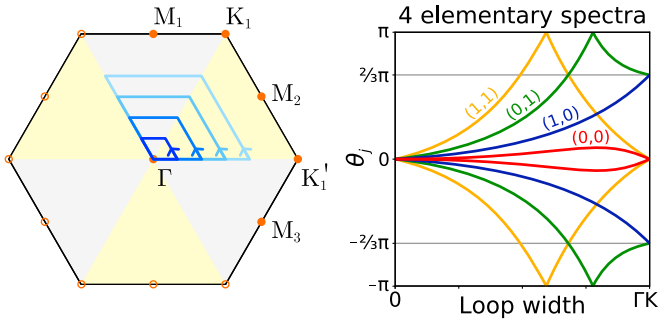

FIG. 1. Left: Concentric Wilson loops in a threefold rotationally symmetric BZ. Right: The corresponding four elementary spectra (schematic), with topological indices indicated as $\mathbf{w} = (w_{\mathrm{FKM}}, w_\pi)$. Spectra with higher winding can be reduced to elementary ones on the addition of a topologically trivial Kramers pair with $\mathbf{w} = (0, 0)$.

pairs, and the associated FKM invariant [2,3,21] may be formulated in terms of a $U(2)$ Wilson loop [22]. In TRS systems without any additional symmetries that cause degeneracies of more than two bands (for instance, due to nonsymmorphic symmetries [23]), it is always possible to consider the $U(2)$ Wilson loop, and more general Berry connections do not contain any additional topological information. We therefore restrict our attention to the $U(2)$ Wilson loops relevant for TRS crystals from here on.

The gauge-invariant Wilson loop eigenvalues of generic closed paths on the Brillouin torus are typically not quantized and do not represent topological invariants [24]. This may be different for paths respecting constraints imposed by symmetry. For instance, the partial polarization in TRS systems is given by the (degenerate) $U(2)$ Wilson loop eigenvalues θ_j along a loop respecting the TRS [5]. Even without such symmetry constraints, however, one can gain topological information by considering a family of generic Wilson loop contours, parametrized by some variable k that collectively yield a spectrum $\theta_j(k)$. For the family of contours in two dimensions with constant crystal momentum component k_x, the parity of the winding of the WLS $\theta_j(k_x)$ equals the FKM invariant [4,5,9].

Here we consider an alternative, "concentric" WLS, which allows us to evaluate not only the generic FKM invariant but also the newly predicted invariant specific to crystals with rotational symmetry. The concentric spectrum consists of loops that do not cycle around the entire BZ torus but instead grow from an infinitesimal loop to enclosing $(1/n)$th of the n-fold rotationally symmetric BZ (see Fig. 1). The gauge-invariant eigenvalues of each of the loops in the spectrum come in pairs of opposite sign and describe the net enclosed $U(2)$ Berry curvature. The spectrum trivially starts at zero (no curvature enclosed) and ends at a value corresponding to $\pm(1/n)$th of the total $U(2)$ Berry curvature present in the BZ. The total winding of the spectrum, times n and modulo 4π, thus equals the FKM invariant. Additionally, we prove in Appendix A in Supplemental Material [20] that linear crossings at $\theta_j = \pi$ can only be gapped by pairwise annihilation. The parity of the number of times the spectrum crosses $\theta_j = \pi$ therefore describes a second topological invariant.

Crossings through $\theta_j = 0$ do not carry the same protection. To see this, consider a spectrum starting and ending at $\theta_j = 0$ with one additional zero crossing in between. This spectrum may be reduced to a completely flat spectrum ($\theta_j = 0$ for all loops in the spectrum) by transformations of the Hamiltonian that do not break any symmetries or constraints. In more general spectra the zero crossings are *fragile*, in the sense that they cannot generally be reduced to a completely flat spectrum by themselves, but the zero crossings can be removed (and the total winding reduced) after adding a trivial Kramers pair and letting the WLS hybridize.

In fact, within each wallpaper group, one can identify a set of concentric WLS whose winding cannot be reduced any further on the addition of topologically trivial, occupied pairs of bands. We call these elementary spectra. See Appendix B in Supplemental Material [20] for details. Figure 1 depicts the elementary spectra for the case of threefold rotational symmetry. These elementary concentric WLS indicate both the FKM invariant, corresponding to the parity of the winding divided by $2\pi/3$ (or $2\pi/n$ for n-fold rotational symmetry) [25], and the new invariant, corresponding to the parity of the number of π crossings.

Threefold rotation. To see how the concentric WLS is used to identify the value of the new invariant in practice, consider a crystal with threefold rotational symmetry (C_3). In systems with C_3 and TRS, the BZ depicted in Fig. 1 hosts four time-reversal invariant momenta (TRIM), namely, Γ and M_i (with $i = 1, 2, 3$ mapped onto one another by C_3). The K points are equivalent and symmetric under C_3, but mapped onto the K' point under the action of the TRS operator T. In contrast to any evenfold rotational group, there is no combination of C_3 with T that returns a state to the crystal momentum $\mathbf{k}$ it started with. Notice also that $T^2 = (C_3)^3 = -1$ because of the spin-one-half nature of electrons. The symmetry-based classification of crystalline topological insulators predicts two $\mathbb{Z}_2$ invariants for these threefold symmetric systems [26]. Accordingly, we can describe all allowed topological phases in C_3-symmetric class AII systems by pairs of numbers $\mathbf{w} = (w_{\mathrm{FKM}}, w_\pi)$. The first of these corresponds to the FKM invariant, and the second is given by the parity of the number of π crossings in this WLS. The latter has not, to the best of our knowledge, been identified before [27].

As an example implementing these invariants, consider a TRS generalization of the Haldane model, given by the Bloch Hamiltonian [28–30]:

$$H = \begin{pmatrix} H^+_{\mathrm{Hal}} & 0 \\ 0 & H^-_{\mathrm{Hal}} \end{pmatrix}$$
$$H^\pm_{\mathrm{Hal}}(\mathbf{k}) = d_1(\mathbf{k})\tau_x + d_2(\mathbf{k})\tau_y + d_3^\pm(\mathbf{k})\tau_z. \qquad (2)$$

Here, τ_i are Pauli matrices for the sublattice degree of freedom, so that, for example, $\tau_x = a^\dagger_\sigma b_\sigma + b^\dagger_\sigma a_\sigma$ with $a^\dagger_\sigma$ and $b^\dagger_\sigma$ creation operators for electrons with spin σ on different sublattices. We also defined $d_1 = \sum_{j=1}^3 [t_1 \cos(\mathbf{k}\cdot\mathbf{a}_j) + t_3 \cos(\mathbf{k}\cdot\mathbf{c}_j)]$, $d_2 = \sum_{j=1}^3 [-t_1 \sin(\mathbf{k}\cdot\mathbf{a}_j) - t_3 \sin(\mathbf{k}\cdot\mathbf{c}_j)]$, and $d_3^\pm = m \pm \sum_{j=1}^6 t_2(-1)^j \sin(\mathbf{k}\cdot\mathbf{b}_j)$. The vectors $\mathbf{a}_j$, $\mathbf{b}_j$, and $\mathbf{c}_j$ connect first-, second-, and third-nearest neighbors [31]. The inclusion of hopping integrals up to third-nearest neighbors allows for phases of H_{Hal} with Chern numbers larger than

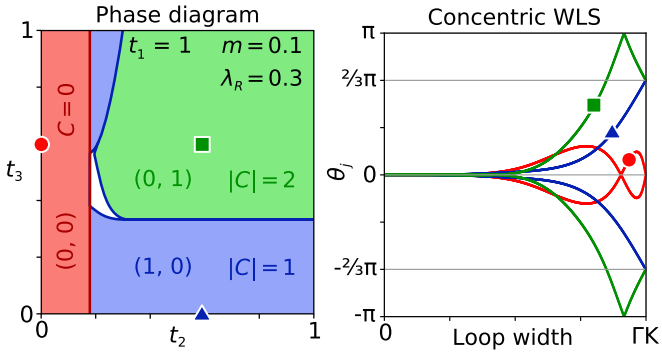

FIG. 2. Left: The phase diagram of the extended Haldane model H_{p3} with $t_1 = 1$, $m = 0.1$, $\lambda_R = 0.3$. The red phase has trivial values for all topological indices, i.e., $\mathbf{w} = 0$. The blue and green phases are nontrivial with their respective $\mathbf{w} = (w_{\mathrm{FKM}}, w_\pi)$ indicated alongside the magnitude of the Chern numbers for $H^{\pm}_{\mathrm{Hal}}$ in each phase. In the white region, the phase could not be unambiguously determined due to (the proximity to) a gap closing. Right: The concentric WLS over one-third of the BZ for the three points indicated by the corresponding symbols in the phase diagram. The values of the two topological invariants for these phases correspond to the parity of $3/(2\pi)$ times the winding of the WLS value, and the parity of the number of π crossings in the spectrum.

one [28–30]. To ensure the system is gapped, we add a Rashba-type spin-orbit coupling connecting the time-reversed elements $H^{\pm}_{\mathrm{Hal}}$:

$$H_{\mathrm{R}} = i\lambda_{\mathrm{R}} \sum_{j=1}^{3} \sum_{\sigma\neq\sigma'} (\mathbf{c}_j \times \mathbf{s})_z^{\sigma\sigma'} e^{i\mathbf{k}\cdot\mathbf{c}_j} a^\dagger_\sigma b_{\sigma'} + \mathrm{Hc}. \tag{3}$$

Here σ is a spin index, $\mathbf{s}$ is the vector of Pauli matrices, and $a^\dagger$ and $b^\dagger$ are again creation operators for electrons on different sublattices. The extended Haldane model Hamiltonian, $H_{p3} = H + H_{\mathrm{R}}$, is invariant under TRS ($T = i\sigma_y \otimes \tau_0 \mathcal{K}$) and threefold rotational symmetry ($C_3 = \exp(i\pi\sigma_z/3) \otimes \tau_0$).

As shown in Fig. 2, the extended Haldane model hosts three distinct topological phases, which can be accessed by varying the relative magnitude of the hopping parameters t_n. The right-hand side of Fig. 2 shows an example spectrum for each phase. The red phase is trivial, having zero total winding and zero π crossings. The blue and green phases are nontrivial and have a total winding that is an odd multiple of $2\pi/3$ and an odd number of π crossings, respectively. Their topological indices are thus $\mathbf{w} = (1, 0)$ and $\mathbf{w} = (0, 1)$. Also indicated are the Chern numbers of the individual $H^{\pm}_{\mathrm{Hal}}$ Hamiltonians, which equal w_{FKM} modulo 2.

Twofold rotation. We now apply the same concentric WLS approach to a TRS system with twofold rotational symmetry. The topological classification for this class of systems was predicted to be $\mathbb{Z}_2^4$ [14,15]. The K theory underlying this classification [32] indicates that two of the $\mathbb{Z}_2$ invariants are *strong* in the K-theory sense of not requiring translational symmetry, while the remaining two invariants do depend on the presence of a periodic lattice [33] (see also Refs. [34,35] for related K-theoretic calculations). These latter two may be interpreted as LBO line invariants along the lines $k_x = 0$ and $k_y = 0$ [6], while one of the strong invariants coincides with the usual FKM invariant. In $p2$, it has recently been shown that a fourth invariant can be identified in systems with trivial FKM invariant [10], which we identify with our new invariant w_π (see also Appendix C in Supplemental Material [20]). These four invariants are independent of one another and cannot be changed on the addition of a trivial band. Topological phases in C_2-symmetric class AII systems can thus be labeled by $\mathbf{w} = (w_{\mathrm{FKM}}, w_\pi, w_{\mathrm{LBO}_x}, w_{\mathrm{LBO}_y})$.

Just as in the case of $p3$, the concentric WLS of systems in $p2$ may always be reduced to four elementary spectra on the addition of trivial occupied Kramers pairs. The complex conjugate eigenvalues of the concentric Wilson loops make up a WLS that always starts at $\theta_j = 0$ and ends at either $\theta_j = 0$ or $\pm\pi$, corresponding, respectively, to $w_{\mathrm{FKM}} = 0$ or 1. As before, zero crossings may be removed (possibly on the addition of a trivial Kramers pair) by flattening the entire spectrum, while π crossings are topologically protected (see Appendix A in Supplemental Material [20]). Notice that this is true even for π crossings in a spectrum of the green type in Fig. 1 (shown for $p2$ in Appendix B in Supplemental Material [20]), which will have a π crossing followed by the spectrum ending at $\theta_j = \pi$. Although the π crossing can be pushed toward the end of the spectrum, it cannot be annihilated and gapped there, because the value at the end of the spectrum equals the FKM invariant, and is quantized. Therefore, the parity of π crossings constitutes a topological invariant even in this special case.

As a generic example of the application of concentric WLS to identify all invariants in twofold symmetric systems, we consider a TRS version of the Qi-Wu-Zhang model [36]. We define the Bloch Hamiltonian:

$$H_{\mathrm{QWZ}}(\mathbf{k}) = d_1\, \sigma_0 \otimes \tau_x + d_2\, \sigma_z \otimes \tau_y + d_3\, \sigma_0 \otimes \tau_z. \tag{4}$$

Here, σ_i and τ_i are Pauli matrices associated with spin and sublattice, respectively. The coefficients are given by $d_1(\mathbf{k}) = \cos k_x$, $d_2(\mathbf{k}) = \cos k_y$, and $d_3(\mathbf{k}) = m^2 - (\sin k_x + \sin k_y)^2$. This Hamiltonian has two chiral symmetries, $C_{x,y} = \sigma_{x,y} \otimes \tau_y$, which we break by adding:

$$H_{\mathrm{int}}(\mathbf{k}) = t_1 \sin k_x\, \sigma_x \otimes \tau_z + t_2 \sin(k_x + k_y)\, \sigma_y \otimes \tau_z. \tag{5}$$

We refer to the full model $H_{p2} = H_{\mathrm{QWZ}} + H_{\mathrm{int}}$ as the QWZ model. It has TRS ($T = i\sigma_y \otimes \tau_0 \mathcal{K}$, with $\mathcal{K}$ complex conjugation) and twofold rotational symmetry ($C_2 = i\sigma_z \otimes \tau_0$). In the following we consider parameter values $t_1 = 1/2$ and $t_2 = 1/10$.

As shown in Fig. 3, the concentric WLS of loops covering half of the BZ indicates that depending on the value of parameter m, the QWZ model resides in one of two phases, with the newly identified invariant $w_\pi = 0$ or 1. In both phases $w_{\mathrm{FKM}} = 0$, while direct computation of the LBO line invariants, equivalent to the value of the (degenerate) WL eigenvalues of loops cycling around the BZ torus with $k_x = 0$ or $k_y = 0$, shows that these are also zero in both phases.

Edge states and corner charges. The bulk-boundary correspondence suggests edge states to be present in finite-sized materials whose bulk Hamiltonian has a nontrivial FKM invariant. Recently, there has been a proposal for a bulk-corner correspondence in rotationally symmetric topological insulators [37]. Intuitively, one expects a minimal requirement for topological corner charges to appear to be the presence

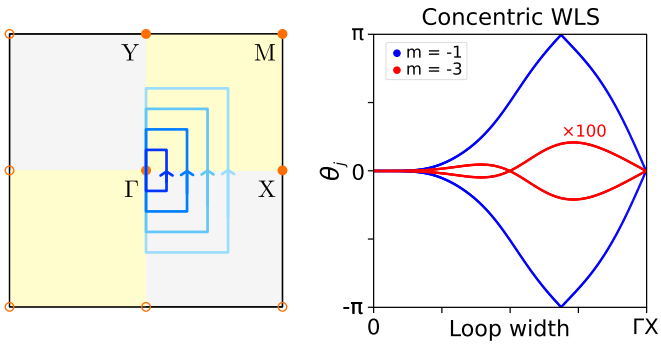

FIG. 3. Left: Concentric Wilson loops covering half the twofold rotationally symmetric BZ. Right: The concentric WLS of H_{p2}, with $t_1 = 1/2$, $t_2 = 1/10$, and two different values of parameter m. The two different topological phases can be described by $\mathbf{w} = (w_{\mathrm{FKM}}, w_\pi, w_{\mathrm{LBO}_x}, w_{\mathrm{LBO}_y})$; red has $\mathbf{w} = (0, 0, 0, 0)$, and blue has $\mathbf{w} = (0, 1, 0, 0)$.

of a winding WLS—indicating the presence of a nontrivial topology—with a trivial FKM invariant such that there are no protected edge states. Such a situation corresponds precisely to the $(w_{\mathrm{FKM}}, w_\pi) = (0, 1)$ phase as seen in the models considered here. To see if this phase indeed hosts corner charges, we consider the extended Haldane model both on a finite-sized hexagon (Fig. 4) and in ribbon configurations with either armchair or zigzag-type edges (see Appendix D in Supplemental Material) [20,38] for the same sets of parameter values as highlighted by the symbols in Fig. 2.

As expected, the $\mathbf{w} = (0, 0)$ phase is a trivial insulator and exhibits no edge or corner states in any configuration. The (1,0) phase hosts topological edge states along both types of edges, as expected for a nontrivial FKM invariant. Interestingly, infinitely long ribbons with zigzag edges in the (0,1) phase also host edge states, while the edge states along ribbons with armchair edges become gapped. The finite-sized hexagon with armchair edges shown in Fig. 4 exhibits fully localized corner charges whose energies lie between those of the gapped edge states.

As discussed in Appendix D in Supplemental Material [20], TRS systems derived from subsystems with odd Chern numbers ($w_{\mathrm{FKM}} = 1$) will always host at least one pair of gapless edge states. Those derived from subsystems with even (nonzero) Chern numbers ($w_{\mathrm{FKM}} = 0$), on the other hand, have no protection against their edge states being gapped. Whether the edge states are in fact gapped depends on the specific geometry of the finite-sized system considered. Even if the system has a gap in both the bulk and the edge state spectrum, the existence of corner charges additionally requires their energies to lie within that gap. Depending on the parameters chosen, corner charges may be pushed into the gapped edge state spectrum and hybridize. A nontrivial value of the newly identified invariant ($w_\pi = 1$) thus signals the possibility of corner charges emerging, but whether they are realized in any specific finite-sized system depends on its detailed configuration.

Discussion. The concentric WLS serves as a single, unified diagnostic allowing the simultaneous evaluation of both the well-known FKM invariant and the topological invariant that were predicted to exist in rotationally symmetric systems based on K-theoretical arguments [15,33]. Complementing the concentric WLS with LBO line invariants, which are given by the eigenvalues of high-symmetry Wilson loops, yields the values of all possible topological invariants appearing in the complete classification of TRS systems with rotational symmetry [15].

We gave explicit examples of this construction for particular tight-binding models in class AII with twofold and threefold rotational symmetries, but stress that the approach is general and can also be applied to cases with higher rotational symmetries, as detailed in Appendix B in Supplemental Material [20]. Combining rotations with additional symmetries, including nonsymmorphic ones, may be expected to further enrich the analysis.

In wallpaper group $p3$, we showed that an odd number of π crossings in the concentric WLS signals the possibility of localized corner charges appearing in finite-sized samples. This may explain the recent observation of corner charges in specific rotationally symmetric systems, which were suggested to be related to a form of fragile topology [37]. Because the parity of π crossings in the concentric WLS is unaffected by the addition of topologically trivial Kramers pairs, the present

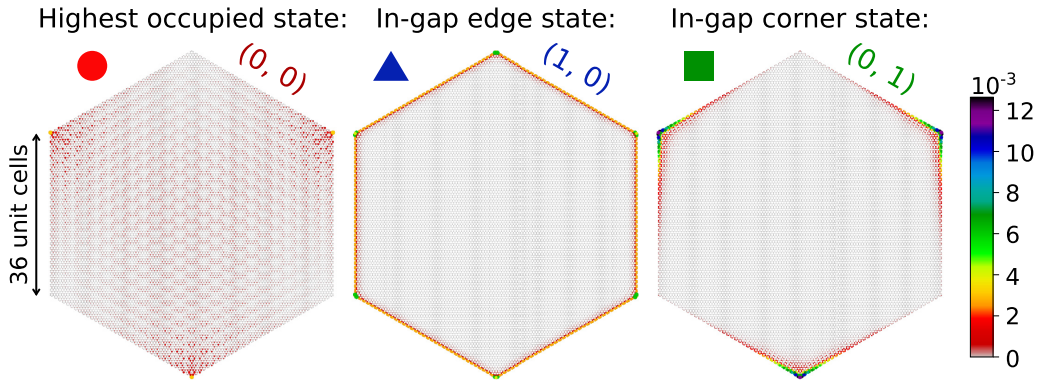

FIG. 4. Exemplary states of the extended Haldane model in a finite-sized hexagon with armchair edges for the three topological phases with parameter values as indicated by the symbols in Fig. 2. The $(0, 0)$ phase hosts no in-gap states, while the $(1, 0)$ phase hosts in-gap edge states and the $(0, 1)$ phase hosts in-gap corner states. The color scale indicates the local density of states, normalized to one in each panel. The states shown lie at $E/t_1 = -0.2$, 0, and -0.05, respectively.

analysis in fact suggests the bulk-corner correspondence in these systems to be stable and described by a true, rather than fragile, topological invariant. While further investigation is required, the existence of this stable invariant is not visible in the usual linear WLS, underlining the utility of the concentric Wilson loops.

[1] D. J. Thouless, M. Kohmoto, M. P. Nightingale, and M. den Nijs, Phys. Rev. Lett. **49**, 405 (1982).

[2] C. L. Kane and E. J. Mele, Phys. Rev. Lett. **95**, 226801 (2005).

[3] C. L. Kane and E. J. Mele, Phys. Rev. Lett. **95**, 146802 (2005).

[4] R. Yu, X. L. Qi, A. Bernevig, Z. Fang, and X. Dai, Phys. Rev. B **84**, 075119 (2011).

[5] A. Alexandradinata, X. Dai, and B. A. Bernevig, Phys. Rev. B **89**, 155114 (2014).

[6] A. Lau, J. van den Brink, and C. Ortix, Phys. Rev. B **94**, 165164 (2016).

[7] F. Schindler, A. M. Cook, M. G. Vergniory, Z. Wang, S. S. P. Parkin, B. A. Bernevig, and T. Neupert, Sci. Adv. **4**, eaat0346 (2018).

[8] A. Bouhon, A. M. Black-Schaffer, and R.-J. Slager, Phys. Rev. B **100**, 195135 (2019).

[9] B. Bradlyn, Z. Wang, J. Cano, and B. A. Bernevig, Phys. Rev. B **99**, 045140 (2019).

[10] S. H. Kooi, G. van Miert, and C. Ortix, Phys. Rev. B **100**, 115160 (2019).

[11] Y. Hwang, J. Ahn, and B.-J. Yang, Phys. Rev. B **100**, 205126 (2019).

[12] A. Bouhon, G. F. Lange, and R.-J. Slager, Phys. Rev. B **103**, 245127 (2021).

[13] G. F. Lange, A. Bouhon, and R.-J. Slager, Phys. Rev. B **103**, 195145 (2021).

[14] J. Kruthoff, J. de Boer, J. van Wezel, C. L. Kane, and R.-J. Slager, Phys. Rev. X **7**, 041069 (2017).

[15] J. Kruthoff, J. de Boer, and J. van Wezel, Phys. Rev. B **100**, 075116 (2019).

[16] H. C. Po, A. Vishwanath, and H. Watanabe, Nat. Commun. **8**, 50 (2017).

[17] H. Watanabe, H. C. Po, and A. Vishwanath, Sci. Adv. **4**, eaat8685 (2018).

[18] R.-J. Slager, A. Mesaros, V. Juričič, and J. Zaanen, Nat Phys **9**, 98 (2013).

[19] A. Alexandradinata, C. Fang, M. J. Gilbert, and B. A. Bernevig, Phys. Rev. Lett. **113**, 116403 (2014).

[20] See Supplemental Material at http://link.aps.org/supplemental/10.1103/PhysRevB.104.L201110 which includes Ref. [39]. The appendices contained therein detail (A) the symmetry constraints on the concentric WLS, which substantiate the extraction of topological invariants; (B) the treatment of more occupied bands and other rotation groups; (C) another example in $p2$; and (D) ribbon bandstructures of the extended Haldane model.

[21] L. Fu and C. L. Kane, Phys. Rev. B **74**, 195312 (2006).

[22] S.-S. Lee and S. Ryu, Phys. Rev. Lett. **100**, 186807 (2008).

[23] S. M. Young and C. L. Kane, Phys. Rev. Lett. **115**, 126803 (2015).

[24] The eigenvalues of any Wilson loop $\mathcal{W}[\mathcal{C}]$ are restricted to being a pure phase $\exp(i\theta_j)$, where j denotes the eigenvalue index. In the text, we use the term "eigenvalue" to indicate the phase θ_j.

[25] To minimize numerical error, we consider a series of concentric hexagonal loops centered at $\mathbf{k}_\Gamma = (0, 0)$ in explicit calculations. We then unfold the spectrum (to access eigenvalues of magnitude larger than $\pm\pi$) and divide the resulting values by three. This is equivalent to considering the spectrum of concentric loops on one-third of the BZ, owing to the threefold symmetry of the $U(2)$ Berry curvature.

[26] This corrects a statement in Ref. [15]: Although $U(1)$ vortices at K cannot be moved, they can be smeared in a C_3 and TRS invariant fashion, leaving two rather than three $\mathbb{Z}_2$ invariants.

[27] Besides the new invariant not having been identified in any model systems on the basis of phenomenological observations, the complete and rigorous K-theory classification for TRS systems with threefold rotational symmetry is, to the best of our knowledge, not known.

[28] F. D. M. Haldane, Phys. Rev. Lett. **61**, 2015 (1988).

[29] D. Sticlet and F. Piéchon, Phys. Rev. B **87**, 115402 (2013).

[30] U. Bhattacharya, J. Hutchinson, and A. Dutta, Phys. Rev. B **95**, 144304 (2017).

[31] Explicitly, $\mathbf{a}_j = (Q_3^T)^j\{0, 1\}^T$, $\mathbf{b}_j = (Q_6^T)^j\{\sqrt{3}, 0\}^T$ and $\mathbf{c}_j = (Q_3^T)^j\{0, -2\}^T$, where Q_3 and Q_6 are three- and sixfold rotation matrices, respectively, and the lattice spacing is set to unity.

[32] D. S. Freed and G. W. Moore, Ann. Henri Poincare **14**, 1927 (2013).

[33] L. Stehouwer, J. de Boer, J. Kruthoff, and H. Posthuma, arXiv:1811.02592 [cond-mat.mes-hall] (2018).

[34] E. Cornfeld and S. Carmeli, Phys. Rev. Research **3**, 013052 (2021).

[35] K. Shiozaki, M. Sato, and K. Gomi, arXiv:1802.06694 [cond-mat.str-el] (2018).

[36] X.-L. Qi, Y.-S. Wu, and S.-C. Zhang, Phys. Rev. B **74**, 085308 (2006).

[37] S. Kooi, G. van Miert, and C. Ortix, npj Quantum Mater. **6**, 1 (2021).

[38] D. Moldovan, M. Anđelković, and F. Peeters, pybinding v0.9.5: a Python package for tight- binding calculations (v0.9.5), Zenodo. (2020), https://doi.org/10.5281/zenodo.4010216.

[39] H. C. Po, H. Watanabe, and A. Vishwanath, Phys. Rev. Lett. **121**, 126402 (2018).